Mössbauer Study of Low-Temperature Anharmonicity in ThO_2 : Co^{57} †

H. Shechter,* J. G. Dash, G. A. Erickson, and R. Ingalls
Department of Physics, University of Washington, Seattle, Washington 98105
(Received 16 December 1969)

A detailed study of the Mössbauer effect of divalent Fe^{57} impurities in ThO_2 shows several remarkable features. Although the most probable impurity sites have nearly cubic symmetry, the spectra have large quadrupole splittings (1.9–2.8 mm/sec). The Debye-Waller factor f is surprisingly low (0.3–0.4), nearly independent of temperature from room temperature to 10 °K. The isomer shift (~1.0 mm/sec re metallic iron) is smaller than the usual value for divalent charge states. All three abnormalities can be explained through the assumption of effective potential wells of the impurities which have a "wine-bottle" shape. Quantitative comparisons based on a simplified "squared wine bottle" with a high central maximum yield an outer radius $R_2 = 0.24$ Å and inner radius $R_1 = 0.19$ Å. The empirical R_2 is comparable with an average "rattle radius" 0.26 Å corresponding to hard spheres with known ionic radii in the ThO_2 structure. Such a model yields f values in close agreement with observations at all temperatures, and a large negative thermal-shift contribution which provides a plausible explanation for the total observed shift. The central maximum of the assumed potential forces the impurity ions into positions of noncubic symmetry, offering a mechanism for the quadrupole splitting. The possibility of a relaxation process is suggested to account for the reduced magnitude of this splitting as well as for the broad lines. Theoretical analysis for f and the thermal shift in spherically symmetric wine-bottle potentials is given, and the occurrence of similar potentials in other impurity systems is discussed.

I. INTRODUCTION

The present work was initiated as a result of recent demonstrations of the utility of the Mössbauer effect in studies of low-temperature anharmonicity.[1–3] As discussed in Ref. 2 a variety of homogeneous and impurity systems contain Mössbauer sites having markedly anharmonic potential minima. The temperature dependence of the Debye-Waller factor f is a sensitive gauge of such anharmonicity. A quantitative theory for relating the temperature dependence of f to the shape of the potential well was used to analyze the results of a study of $FeCl_2$.[3] Substantial agreement was found between the well parameters resulting from the Mössbauer study and a simple model based on the relative sizes of the ions in the crystal.

Thorium oxide is a highly refractory material with a melting point above 3000 °C and correspondingly strong force constants.[4,5] Thus if Co^{57} could be introduced substitutionally for Th as an impurity in ThO_2, and if the impurity-host binding forces were comparable to host-host binding, we would expect a Debye-Waller factor f approaching unity even at room temperature. On the other hand, if the effective potential near the minimum is primarily determined by the separation and hardness of ionic cores, then the small size of the iron ion relative to thorium would produce an abnormally low f and anharmonic behavior at low temperatures.

This paper describes a Mössbauer study which provided a quantitative test and an elaboration of the previous studies of low-temperature anharmonicity.

II. EXPERIMENTAL

Optical and ESR studies (see Sec. V A) have shown that ThO_2 crystals can be grown with appreciable concentration of cation impurities, including Fe. These results indicate that the impurities are Fe^{2+} in sites of essentially cubic symmetry, and hence are presumably substitutional or quasisubstitutional for the Th^{4+}. We found thermal diffusion of Co^{57} at moderate temperatures (~600° C) to be sufficiently rapid to allow innoculation of several single-crystal and polycrystalline ThO_2 host materials.[6–9] The basic preparation for each source consisted of (a) doping the material with 0.1N Co^{57} Cl_2 in H_2O solution prepared commercially,[10] (b) baking under vacuum or partial H_2 atmosphere at 575–600 °C for 15–20 min, (c) washing with HCl and distilled H_2O, and (d) abrading the surface with emery paper when feasible. The ratios of 14-keV radiation to high-energy background [from 122-keV peak mainly (>95%)] were used as an indication of the averaged diffusion depth, typically on the order of 0.1 mm.

Samples were prepared by the above technique from an optically pure single crystal,[6,7] powder,[8] and a sintered pellet.[9] The spectra of these sources were identical within experimental error at room temperature. The f values of the polycrystalline

sources were reduced from those of the single crystal by about 5–15%. We feel that this was due to nondiffused activity remaining on the crystal surfaces as it was impossible to abrasively clean the polycrystalline faces. The f values of the polycrystalline sources were increased by 15% at all temperatures to compensate, a correction we feel is conservative in that it decreases the degree of low-temperature anharmonicity.

In order to study the temperature dependence of the sources, they were mounted in the sample holder of a cryostat. The sample holder was rigidly clamped against vibrations without thermally linking the sample to room temperature.[11] Temperatures of the samples were stable to within 0.5 °K at all temperatures over a 24-hour period. The various absorbers were mounted on a mechanically coupled speaker pair driven in a linear velocity mode. Counts were stored in a Nuclear Data Model 130 multichannel analyzer operating in coincidence mode.

III. MEASUREMENTS AND PROCEDURE

A. Procedure

A detailed background analysis was carried out by previously described techniques.[3,12,13] We measured the fraction of the $ThO_2:Co^{57}$ sources with an enriched wide absorber (EWA) by comparison of absorption areas of several known sources and by an "on-off" technique described elsewhere.[12] The latter was valuable even in our case of broad emission lines for two reasons: It allowed us to compare effects of geometry with the sample in and out of the cryostat, and it gave us the ratios, $I(\infty):I(0):I$(background), as a check on the velocity spectra of the ThO_2 source versus the EWA.

The technique of relative f measurements via absorption area was the best suited for $ThO_2:Co^{57}$ with its broad emission lines, because the area of the velocity spectrum is independent of the source line shape or velocity-independent instrumental broadening and is only weakly dependent on the absorber line shape.[12] When an area comparison is made between the spectra of two sources, the effect of the absorber is eliminated, being the same for both. Where one of the source fractions is known absolutely in a relative measurement, all comparative fractions are determined absolutely. Thus, we chose the EWA for the comparison absorber because of the magnitude of its effect, and we chose to compare the ThO_2 sources to the $Cu:Co^{57}$ copper source previously studied in this laboratory.[14]

The Mössbauer fraction for $ThO_2:Co^{57}$ was given by

$$f_{ThO_2:Co} = f_{Cu:Co} \times (A_1/A_2) \times (R_2/R_1), \qquad (1)$$

where A_1 is the absorption area of velocity spectrum $ThO_2:Co^{57}$ versus EWA, A_2 is the absorption area of velocity spectrum $Cu:Co^{57}$ versus EWA, R_2 is the percent of 14-keV radiation of the $ThO_2:Co^{57}$ spectrum, and R_2 is the percent of 14-keV radiation of the $Cu:Co^{57}$ spectrum

Velocity spectra of $ThO_2:Co^{57}$ sources were taken versus the EWA along with measurement of $I'(\infty)$, $I(0)$, and I' (background) at all temperatures studied. In order to study the emission line shapes of the ThO_2 sources, velocity spectra were taken versus a single line enriched $Na_4Fe(CN)_6 \cdot 10H_2O$ absorber.[15] Velocity calibration of the spectrometer was performed via the above Cu source versus Armco natural iron foil spectrum for each run.

B. Results

Figure 1 is a representative spectrum of $ThO_2:Co^{57}$ versus the enriched $Na_4Fe(CN)_6 \cdot 10H_2O$ absorber. The emission spectra at all temperatures studied are resolvable into two very broad dips of weak intensity. The spectra were approximately fit by a computer program using Lorentzian lines,[16,17] Fitting was attempted with 2, 3, 4, and 5 lines. None of the fits appeared to be consistent at all temperatures. The best approximate fits were generated for a pair of lines with identical half-width and intensity and a small third peak located between these with broader half-width. The approximate velocity positions of the pair and the third peak led us to associate quadrupole split Fe^{2+} ions with the pair and Fe^{3+} ions with the third peak. The

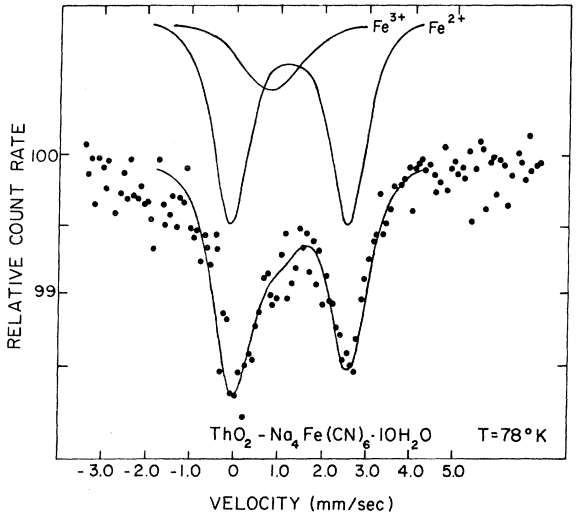

FIG. 1. Velocity spectrum of ThO_2 #3 versus enriched $Na_4Fe(CN)_6 \cdot 10H_2O$ at $T = 78$ °K. Positive velocity is defined for the absorber moving away from the source. A theoretical fit from the relaxation calculation shown is by the solid curve. The Fe^{2+} and Fe^{3+} components are identified above the fit. Velocity defined as in Fig. 1.

area ratios of the peaks lead us to conclude that the iron impurities are about 66% divalent and 33% trivalent. No evidence for other charge states could be found. The poor computer fit, broad lines of weak intensity, and reduced value for the quadrupole splitting led to a set of fits incorporating relaxation broadening, which we discuss later, enabling us to fit the spectra more consistently. The solid lines are the fit to the spectrum in Fig. 1 by the calculation allowing for the Fe^{2+} and Fe^{3+} components. The half-widths of all three lines were relatively independent of temperature to within statistical uncertainty in the range of 1.2 ± 0.2 mm/sec for Fe^{2+} and 1.4 ± 0.3 mm/sec for Fe^{3+}. The velocity shift of the Fe^{2+} component shows a very weak temperature dependence [Fig. 2(a)].

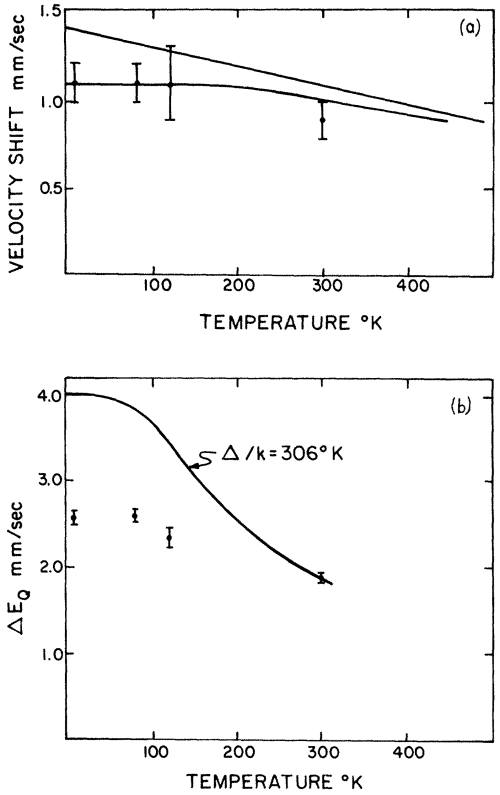

FIG. 2. (a) Velocity shift (isomer shift) of the Fe^{2+} component versus temperature. The solid lines are curves for the velocity shift of a wine-bottle potential with hard central maximum with a chemical shift of 1.4 mm/sec. The upper curve is the high-temperature classical behavior extrapolated to low temperatures; the lower curve is the isomer shift corresponding to potential well radii of $R_2 = 0.245$ Å and $R_1 = 0.195$ Å or, equivalently, the ground-state energy of $\zeta_1/k = 600$ °K. (b) Quadrupole splitting of the Fe^{2+} component versus temperature. The solid line is calculated from the equation $\Delta E_Q(T) = \Delta E_0 \tanh(\Delta/2kT)$ with $\Delta E_0 = 4.0$ mm/sec and $\Delta/k = 306$ °K.

The chemical shift from the room-temperature isomer shift is $\sim 1.2 \pm 0.1$ mm/sec, which is reduced from the expected shift for ionic Fe^{2+} in eightfold symmetry.[18,19] Owing to the small intensity and large half-width, the isomer shift of the Fe^{3+} component illustrates no observable temperature dependence. All the values are in the range of $\delta v = 0.3 \pm 0.2$ mm/sec. The quadrupole splitting of the Fe^{2+} component varies from 1.88 ± 0.05 mm/sec at room temperature to 2.57 ± 0.05 mm/sec at $T = 10$ °K[Fig. 2(b)]. The quadrupole splitting at all temperatures is substantially weaker than the expected value for ionic divalent Fe^{57} in the case of very slow relaxation, where $\Delta E_Q = \Delta E_O (\sim 4.0$ mm/sec) for all temperatures.[18] The temperature dependence also shows marked deviation from fast relaxation behavior, which is characterized by $\Delta E_Q = \Delta E_O \tanh(\Delta/2kT)$, where Δ is the electronic orbital splitting (see Sec. V C).

The Mössbauer fraction exhibits abnormally weak temperature dependence, varying from $f = 0.30$ at room temperature to $f = 0.41 \pm 0.02$ at $T = 10$ °K. These results are shown graphically in Fig. 3. They are compared with theoretical curves based on an Einstein model with characteristic temperature of $\Theta_E = 107$ °K, and a Debye model with $\Theta_D = 185$ °K, both curves being matched to the measured f at room temperature. The deviation of the experimental values from these curves is quite marked. Table I summarizes the relevant data at each temperature.

IV. PRELIMINARY ANALYSIS: HARMONIC FORCES

The experimental results for f, ΔE_Q, and the isomer shift are all abnormal in that they show considerable departures from the values or temperature dependences of convential models. Of the three experimental quantities f is the most anomalous and also provides the strongest clues toward the development of a plausible and comprehensive model. In Sec. IV we compare the magnitude and temperature dependence of f with the behavior of simple harmonic substances.

The simplest treatment for the f of impurities is to assume them to be bound harmonically with the characteristic force constants of the host, i.e., to treat them as simple "isotopic" impurities. Two roughly equivalent methods for the practical prediction of f are available: the theories of Lipkin[20] and of Dawber and Elliott.[21] In both theories it is shown that the isotopic impurity f can be closely estimated by adjusting the characteristic temperature of the host by the square root of the impurity-to-host atomic mass ratio. If we do assume that the Fe^{57} ions are isotopic substitutional impurities, then with the measured characteristic Debye temperature $\Theta_D = 394$ °K of pure ThO_2,[22] the character-

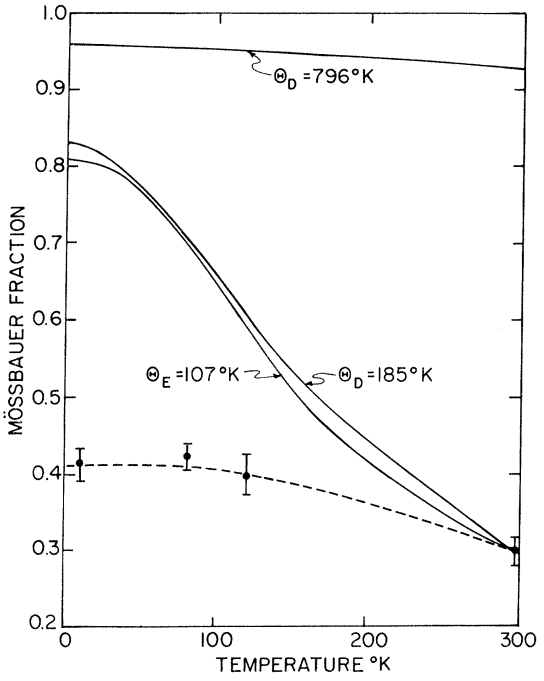

FIG. 3. Mössbauer fraction of ThO_2:Fe^{57} versus temperature. The solid lines are calculated from an Einstein model of the frequency distribution with characteristic temperature $\Theta_E = 107$ °K and from a Debye model with characteristic temperatures $\Theta_D = 185$ °K and $\Theta_D = 796$ °K.

istic temperature of the impurities is (scaling according to the mass ratios of Fe^{57} and Th^{232}) $\Theta_{imp} = 796$ °K. Corresponding f values calculated according to the usual Debye formula are

$$f_{imp}(300\ °K) = 0.93 \quad f_{imp}(0\ °K) = 0.96.$$

We may also compare the f with values corresponding to an impurity having a δ-function (Einstein) frequency distribution. Such a model might be a reasonable one for the relatively light impurities, which can be expected to vibrate in a localized high-frequency mode.[23] The Einstein model also affords a greater degree of flexibility in that it is possible to normalize the f to the experimental value at one temperature, thereby fixing the value of the effective force constant acting on the impurity. If this is done, normalizing at room temperature, then we find the calculated value at 0 °K to be 0.815. A graphical comparison of the data with both of the above calculations is given in Fig. 3.

The Einstein model has a special significance. Housley and Hess[1] have shown that if f is normalized to data at a single temperature, then an Einstein model provides the lowest possible value of f (0 °K) afforded by any distribution of harmonic modes. Therefore, we find that the temperature dependence of f implies a considerable degree of anharmonicity of Fe^{57} in ThO_2. In Sec. V we inspect the data in greater detail and compare the results with a specific anharmonic model.

V. DETAILED ANALYSIS

A. Impurity sites

The crystal structure of ThO_2 is isomorphous to CaF_2. Figure 4 is a perspective packing drawing showing the distribution of Th^{4+} and O^{2-} within a unit cell.[24] The oxygen ions form a simple cubic lattice. Each Th^{4+} is found at the center of a cube of eight O^{2-} ions at the corners and each oxygen is found at the center of a tetrahedron of thorium ions. The impurity structure of this material has been previously discussed since its physical properties are often measured via impurity atoms. It was found by ESR studies[25] that the cubic symmetry of ThO_2 is present to a high order with impurity trivalent gadolinium, despite the fact that the Gd^{3+} has a smaller size than the atoms in the host lattice. It was suggested that symmetric charge distributions (S states) attract nearest neighbors uniformly and prevent the formation of vacancies or associated interstitials in the neighborhood of the impurity.

It was shown by Hund and Durchwachter[26] by x-ray analysis that in a high-purity crystal of ThO_2 there are some negative vacancies randomly distributed throughout the crystal. Recently, optical and ESR studies showed[8] that in single crystals of ThO_2 being subjected to ionizing radiations, there is local tetrahedral symmetry which is very slightly distorted

TABLE I. Experimental data for ThO_2:Fe^{57}.

Temp. (°K)	Fraction f	Half-width Γ mm/sec Fe^{2+}	Velocity shift δv mm/sec Fe^{2+}	Qudrupole split ΔE_Q mm/sec	Half-width Γ mm/sec Fe^{3+}	Velocity shift δv mm/sec Fe^{3+}
10.6±0.5	0.41±0.02	1.4±0.2	1.1±0.1	2.57±0.05	1.5±0.3	0.3±0.3
78.0±0.5	0.42±0.02	1.2±0.2	1.1±0.1	2.60±0.05	1.5±0.3	0.5±0.3
120.0±0.5	0.39±0.03	1.0±0.3	1.1±0.2	2.35±0.1	1.8±0.5	0.3±0.4
298.0±0.5	0.30±0.02	1.1±0.2	0.9±0.1	1.88±0.05	1.0±0.3	0.5±0.3

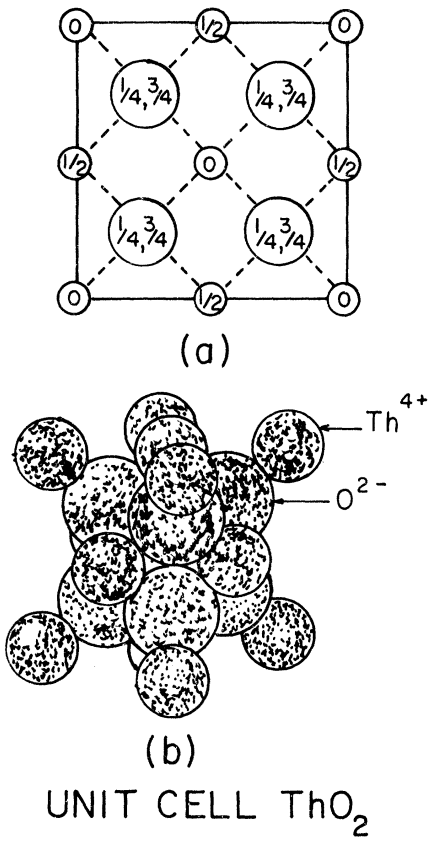

FIG. 4. (a) Perspective packing drawing of the positions of the ions in the unit cell of CaF_2-type structure. The oxygen ions of ThO_2 occupy the $\frac{1}{4}$, $\frac{3}{4}$ positions and the thorium ions occupy the 0, $\frac{1}{2}$ positions. (b) The unit cell of ThO_2 with the ions given their relative sizes.

axially along the body diagonal in the over-all cubic symmetry of the ThO_2 lattice. These vacancies play an important role in the electric field gradient (EFG) considerations and in the charge-neutrality mechanism of the crystal in the presence of impurity ions. ESR results[25] indicate that the oxygen vacancies are probably not localized in the immediate neighborhood of the impurity ion. In determining the location of the cobalt impurity in the host ThO_2 we have to meet several restrictions: (i) The Mössbauer patterns suggest the presence of divalent and trivalent cobalt. (ii) The cobalt ions are substitutional for thorium ions or interstitial in the Th substructure.[27] (iii) The ThO_2 remains electrically neutral on the average. (iv) The low f implies ample rattling space for the cobalt ions. (v) The similarity of the spectra for the single-crystal and polycrystalline sources indicates the bulk of the diffused Co^{57} is not influenced by crystal defects. We have no means for accurately determining the number of oxygen vacancies in our samples, However, if the mechanism for charge compensation for impurities is taken care of by oxygen (as suggested by Low and others), the concentration of oxygen vacancies deduced from similar cases in the literature is of the same order of magnitude as required for our sample, i.e., assuming that the 0.7 mC of radioactive cobalt ($\sim 10^{15}$ nuclei) are charge compensated by oxygen vacancies for the known active volume ($\sim 10^{-4}$ cm^3). The ratio of Co^{2+} to Co^{3+} is 2:1 from the relative intensities in the emission spectra. A simple calculation shows that the average distance between two cobalt ions in the sources is about 15 lattice parameters, and for Mössbauer purposes it is dilute.

B. Recoil-free Fraction and Thermal Shift

Dash *et al.*[2] have shown that for an arbitrary degree of low-temperature anharmonicity, factorization of f is a reasonable approximation at all temperatures:

$$f = f_{\text{host}} \times f_{\text{loc}} \quad , \tag{2}$$

where f is the measured f of impurity, f_{host} is the f binding local well to harmonic solid, and f_{loc} is the f due to shape of local well.

The relatively strong force constants of pure ThO_2 indicate that $f_{\text{host}} \simeq 1$ over the explored temperature range. We can then assume as a first approximation that the experimental f is essentially equal to f_{loc}. If we now assume for the local potential a simple spherical cavity,[2] we can approximate the magnitude and temperature independence of f with a cavity having an effective radius of 0.215 Å. However, the thermal shift implied by this radius appears too small to account for the total observed shift. It appears that the observed line shift is at least 0.2 mm/sec smaller than can be accounted for by the chemical shift of divalent impurities. Furthermore, the high symmetry of a simple spherical cavity allows no mechanism for the large splitting. Although one does not usually attempt to explain f, shift, and splitting through the assumption of a potential well of special and unusual shape, we do find it possible to explain all three in this material.

The potential suggested by f, shift, and splitting has a spherical wine-bottle shape. Wine bottle is a term first used by Elsasser[28] to describe potential wells having central maxima. Such wells were for several years believed to characterize single-particle potentials in heavy nuclei,[29] but have since been replaced by complex potentials with simpler spatial dependences. There are several atomic systems which appear to have wine-bottle potentials, including dense gases and simple liquids,[30] solid helium,[31] clathrate compounds,[32] and small sub-

stitutional impurities in ionic crystals.[33] Co^{57} in ThO_2 can be expected to resemble the last class of materials owing to the relatively small size of the Fe ion in the ThO_2 sites. Detailed studies of small substitutional impurities in ionic crystals have given evidence of subsidiary minima distributed about the central maximum. However, we presently have no evidence for subsidiary minima in $ThO_2:Co^{57}$, and therefore have assumed the simpler shape of a spherically symmetric hard-walled cavity having a strong and hard central maximum [Fig. 5(c)]. The detailed calculation of the Debye-Waller factor and thermal shift for such a potential is given in the Appendix. Parameters yielding the best fit to the measured values f ($T \leq 10$ °K) $= 0.43$ and $\delta v = -0.3$ mm/sec are

outer radius $(R_2) = 0.245 \pm 0.005$ Å,

inner radius $(R_1) = 0.195 \pm 0.005$ Å.

C. Quadrupole Splitting

The above suggested model also allows one to postulate a mechanism leading to an explanation for the observed quadrupole splitting. In an attempt to fit theoretical curves to the velocity spectra, several approximate Lorentzian fits were obtained that were consistent for the various temperatures. The two dips appear resolvable into a quadrupole split doublet which we associate with the Fe^{2+} ions. The approximate values obtained for the quadrupole splitting, the broad linewidth, the weak temperature dependence of the isomer shift, and poor computer fit then suggested the possibility of a quadrupolar relaxation process which we discuss below.

As discussed earlier, we assume that the Fe^{2+} ion is either substitutional for Th^{4+} or else in one of the vacant sites (body center of the fcc Th^{4+} sublattice). In either case, it is surrounded by a cube of eight O^{2-} ions, i.e., it has eightfold coordination (fluorite structure, Fig. 4). The observed quadrupole splitting ΔE presumably can come about by a static perturbation of the perfect cubic symmetry by any of the following: nearby charge compensation, distortion of the O^{2-} cube, or with the ferrous ion in an off-center position. In cubic symmetry, it can also come about through a slow relaxation between members of a spin-orbit multiplet or by means of a dynamic Jahn-Teller effect as discussed below.

In eightfold coordination the atomic ^5D state of the Fe^{2+} ion is split into a low-lying orbital doublet $^5\Gamma_3$ and an orbital triplet $^5\Gamma_5$, some 10^4 cm^{-1} higher in energy.[34] One expects the splitting in eightfold coordination to be about the same as the splitting found in a sixfold (octahedral) coordination, namely, 10^4 cm^{-1}, for a near-neighbor distance of 2.1 Å. In the present case, the nearest-neighbor distance is 14% greater than the usual octahedral spacing. Thus it is possible that the $\Gamma_3 - \Gamma_5$ cubic splitting Δ_0 is reduced to perhaps 4000 cm^{-1}. Spin-orbit coupling to the Γ_5 levels splits the Γ_3 levels in second order by $24\lambda^2/\Delta_0$ or ~30–60 cm^{-1}, where $\lambda(\sim 10^2$ cm$^{-1})$ is the spin-orbit parameter. This is in marked contrast to the octahedral case where the lowest orbital Γ_5 is split in first order by 5λ or ~500 cm^{-1}.[34]

The two Γ_3 orbitals transform as $|x^2 - y^2\rangle$ or $|3z^2 - r^2\rangle$. Any of the perturbations mentioned earlier can remove their degeneracy, and if greater than the spin-orbit perturbation, the two re-

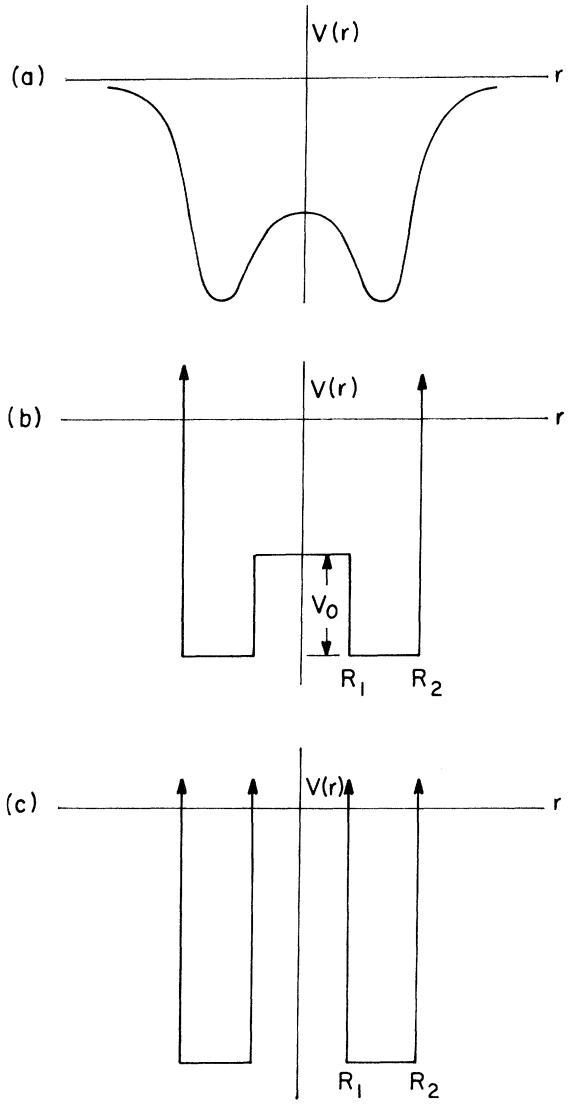

FIG. 5. (a) Typical radial dependence of a wine-bottle potential. (b) Radial dependence of a squared wine-bottle (SWB) potential. (c) Radial dependence of SWB potential with hard central maximum.

sulting orbital wave functions may be represented in first order by

$$\psi_+ = \cos\alpha\ |x^2-y^2\rangle + \sin\alpha\ |3z^2-r^2\rangle\ ,$$

and (3)

$$\psi_- = -\sin\alpha\ |\ x^2-y^2\rangle + \cos\alpha\ |3z^2-r^2\rangle\ .$$

Using the usual definition, neglecting a lattice contribution,

$$V_{zz} = eq = -e\left\langle \psi_\pm \left| \frac{3\cos^2\theta - 1}{r^3} \right| \psi_\pm \right\rangle = \frac{\pm 4e}{7}\left\langle \frac{1}{r^3}\right\rangle \cos 2\alpha,$$

$$V_{xx} - V_{yy} = eq\eta = -e\langle \psi_\pm |\, 3\sin^2\theta\cos^2\phi\ |\psi_\pm\rangle = \pm\frac{4\sqrt{3}\,e}{7}\left\langle \frac{1}{r^3}\right\rangle \sin 2\alpha. \quad (4)$$

The quadrupole splitting due to either orbital state is thus

$$\Delta E_0 = \tfrac{1}{2}e^2qQ(1+\tfrac{1}{3}\eta^2)^{1/2} = (2e^2Q/7)\langle 1/r^3\rangle\ , \quad (5)$$

less, perhaps, some 1% by split-orbit coupling. This is in marked contrast to the octahedral case, where spin-orbit effects can reduce the orbital contribution appreciably.[35] If the two states have a probability difference $p = |p_+ - p_-|$ and there is rapid relaxation between them, then the quadrupole splitting is $\Delta E = \Delta E_0 p$. For the usual case the probabilities are Boltzmann factors and $p = \tanh(\Delta/2kT)$, where Δ is the splitting between the two states.[36] For ionic Fe^{2+} octahedral complexes, the factor $\Delta E_0 = \frac{2}{7}e^2Q\langle 1/r^3\rangle$ varies from 3.5 mm/sec for Fe^{2+} in MgO, to 4.1 mm/sec for Fe^{2+} in $FeSiF_6 \cdot 6H_2O$.[18] [The room-temperature isomer shifts (IS) vary from 1.0 to 1.4 mm/sec, respectively, with respect to metallic iron.] In the present case such an analysis of the spectrum yields $\Delta E_0 = 2.8$ mm/sec (and IS = 1.1 mm/sec).

The above expression $\Delta E = \Delta E_0 \tanh(\Delta/2kT)$ has been used to explain the quadrupole splitting of Fe^{2+} in tetrahedral symmetry[36,37] in which the Γ_3 state is also lowest. In these cases the parameter ΔE_0 is in the range 2.8–3.2 mm/sec and the isomer shifts are approximately 0.8–1.0 mm/sec. It is somewhat doubtful that covalency, spin-orbit effects, or lattice EFG contributions can entirely account for these small values of ΔE_0. A more reasonable explanation[36] is that there is a configuration interaction causing some $4p$ admixture. Low and Weger[34] have stressed the importance of such an effect in cases with no inversion symmetry, such as tetrahedral symmetry.

Although the values of IS and ΔE_0 for the ThO_2 case are similar to the tetrahedral cases above, the deviation (reduction) from ionic, octahedral behavior is yet more pronounced, even in the presence of inversion symmetry. Our linewidths are also much greater than in the tetrahedral cases. Moreover, the simple impurity potential model can predict an anomalously strong thermal shift, large enough to explain the IS reduction. It has recently come to our attention that Fe^{2+} in highly doped CaF_2[19] (to our knowledge the only other experiment of Fe^{2+} in eightfold symmetry) yields IS and ΔE values which are slightly larger than the greatest found in octahedral cases, namely, $FeSIF_6 \cdot 6H_2O$.[18] For the above reasons we consider a model of slow relaxation as a possible alternative to covalency and configuration interaction in order to explain our spectra.

A modification on the above crystal-field treatment of two ionic levels is to assume that the relaxation time τ associated with transitions between Ψ_+ and Ψ_- is comparable with the quadrupole precession time. The theory for such a process has been given by several authors.[38-40] Qualitatively, the resulting spectra may be described in several regimes (Fig. 6). For very short times, one obtains narrow lines and a splitting $\Delta E = \Delta E_0 p$ as shown previously. For very long times, narrow lines are obtained, but $\Delta E = \Delta E_0$, independent of the probability difference p, since the ion is in either Ψ_+ or Ψ_- during the γ-ray emission, and either state produces the same

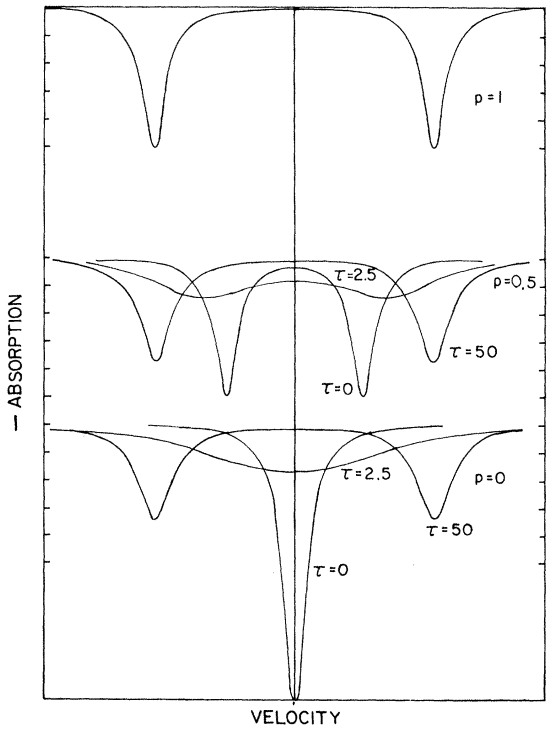

FIG. 6. Emission spectra for various probability differences p and relaxation times τ.

splitting. For intermediate relaxation times with $p \simeq 1$ one finds narrow lines and $\Delta E \cong \Delta E_0$. However, at lower values of p there is considerable line broadening. Moreover, in this intermediate case ($p<1$) the splitting is greater than $\Delta E_0 p$ but less than ΔE_0.

Assuming a value $\Delta E_0 = 4.0$ mm/sec corresponding to a relatively ionic case, it is possible to fit the Fe^{2+} component with values of τ on the order of 10^{-9} sec, which decrease with increasing temperature; we also find $p \sim 0.5$ with little temperature variation (Fig. 7). The errors on τ are sufficiently great to limit extensive critical analysis, however, the dependence of p upon T is sufficiently accurate to rule out either the possibility of strict Boltzmann population and constant Δ, or equal probabilities ($p = 0$).

If Δ is permitted to vary with T in order to assign a Boltzmann interpretation to p, i.e., $p = \tanh(\Delta/2kT)$, then Δ would have to roughly equal kT to give the observed dependence. If the splitting Δ were due to some charge compensation, the latter would be roughly 20 Å away at 10 °K and its distance would decrease to within 7 Å at 300 °K, an unlikely possibility. However, if the splitting were due to the Fe^{2+} being displaced off center, it would be displaced by ~0.05 Å at 10 °K and ~0.3 Å at 300 °K. The latter behavior is also probably too extreme, but is not entirely ruled out.

It is also possible to obtain fits to the spectra with $\Delta E_0 = 3.0$ mm/sec, corresponding to a high degree of covalency (not shown). In this case, the lifetime parameter τ turns out to be roughly three times greater at all temperatures than for $\Delta E_0 = 4.0$ mm/sec, but the factor p then increases with increasing T, although its uncertainty is very large. In Sec. VI we include a discussion of the types of motion which could give the observed quadrupolar relaxation and also again briefly touch upon the probability factor p.

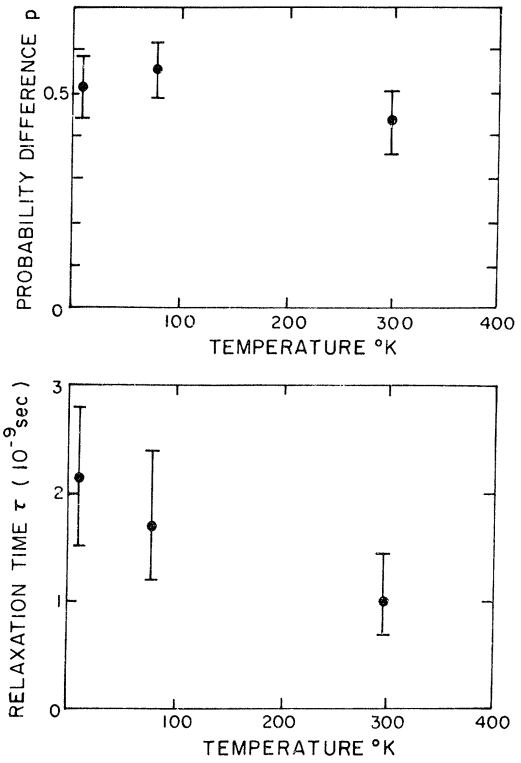

FIG. 7. Temperature variation of probability difference p and relaxation time τ fit to experimental spectra.

VI. DISCUSSION

We have assumed that the anharmonicity is limited to the interactions between certain atoms and their immediate neighbors, while the remaining interactions in the crystal are essentially harmonic. The close-packed array of relatively large oxygen ions together with the low f suggest that the size of the cage around the cobalt impurity is not limited by the overlapping cobalt-oxygen clouds, but rather by oxygen-oxygen electron clouds overlapping. The cobalt nearest-neighbor force constant may be influenced by the electrostatic and covalent forces. The latter will add an attraction nonlinear with the separation, and this will tend to drive the cobalt toward one of its oxygen neighbors; the purely electrostatic effects may also tend to make the center of symmetry a position of a stable equilibrium. Because of the short-range nature of the overlap forces, the destabilizing forces acting on the cobalt ion can dominate at the center of symmetry and lead to minima near the oxygen ions. If the energy barriers between these minima are not greater than kT or the zero point energy, the cobalt will not be trapped at any of the positions and the dynamic center will still be at the center of symmetry. Accordingly, the cobalt ions will move in a very nonharmonic potential at "low" temperatures, and the mean-square displacement will be larger at low temperatures than expected on the basis of harmonic analysis of the high-temperature results.

We find that the empirical outer radius (R_2) of the wine-bottle potential is an approximate agreement with a hard-sphere model. Using the known unit-cell dimensions of ThO_2[24] and ionic radii 1.00 Å for Th^{4+}, 1.40 Å for O^{2-}, and 0.74 Å for Fe^{2+}, the calculated "rattle space" for Fe^{2+} is 0.26 Å. This agrees rather well with the empirical R_2 of 0.245 ± 0.005 Å.

This model has the further feature that, with the center of symmetry a point of astable equilibrium, the potential will lift the cubic-type degeneracy of the impurity ion, splitting the Γ_3 electron-

ic state. This we feel provides the basis for a relaxation process leading to the broad emission lines and reduced low-temperature quadrupole splitting which we observe. The relaxation formula we have used in fitting the spectra is, however probably oversimplified, since it is based upon a static splitting between the two orbitals Ψ_+ and Ψ_-; yet it permits a reasonable interpretation to the gross features of the data in terms of two parameters, relaxation time τ, and probability difference p.

In view of the anomalously large mean-square displacement, it is thus fair to question the notion of a deviation from cubic symmetry and resulting crystal-field splitting in order to see such a large quadrupolar interaction. One can imagine the Fe^{2+} ion undergoing several types of motion which give a time-varying Δ. The ion would see an average Δ, which might have considerable temperature dependence, especially if the character of the motion changes with temperature. For example, if the motion were like an s state (Γ_1), one would expect Δ to vanish. The same would apply to a triply degenerate motion like a p state (Γ_4). However, if only one member of the Γ_4 triplet were populated, as in linear motion along one axis, or if two members were occupied, as in circular motion (wine bottle), one would see a nonvanishing Δ. Thus if the motion were Γ_1 at low temperature and Γ_4 at high temperatures, one would see Δ increase with temperature. This could possibly explain the temperature dependence of the probability factor p. Of course, there are also many possibilities of temperature-dependent relaxation between these modes. A more general three-axis relaxation[39] model would then probably bypass the somewhat artificial problem of the factor p and splitting Δ.

Another possibility is a dynamic Jahn-Teller effect.[41–43] The qualitative behavior would be much the same as discussed above. Such a case, of course, contributes to the quadrupole splitting of Fe^{2+} in MgO although the main cause is relaxation between strain-split Γ_5 spin-orbit levels.[41] In principle, a behavior similar to the latter would yield much larger quadrupole splittings in the present case where the Γ_3 state is lowest,[44] but it seems unlikely that such a splitting would then persist to room temperature.

ACKNOWLEDGMENTS

We are pleased to acknowledge the early advice and suggestions of Professor J. B. Gruber of Washington State University, in the choice and treatment of the host material. We are also indebted to Dr. F. S. Ham and Dr. M. Blume for discussions on the relaxation phenomenon. We wish to extend our gratitude to Dr. N. Gregory of the University of Washington and T. Chikalla of Battelle at Richland for furnishing us with excellent host materials. Two of us (H. S. and R. I.) gratefully acknowledge partial support from the U. S. Atomic Energy Commission.

APPENDIX: f AND $\delta\nu$ FOR A SIMPLE WINE-BOTTLE POTENTIAL

A spherically-symmetric wine-bottle potential has the general shape shown qualitatively in Fig. 5(a). A simplification, for calculations of the Debye-Waller factor f and thermal shift $\delta\nu$, is afforded by the squared wine bottle, illustrated in Fig. 5(b). We will base our calculations of both quantities on this simplified single-particle potential for the "classical" high-temperature regime. For low temperatures, we further simplify the calculation by assuming a very strong central maximum [Fig. 5(c)]. Thus, we base the calculations on an assumed form:

$$\begin{aligned} &V(r) = V_0, \quad 0 < r < R_1 \\ &V(r) = 0, \quad R_1 < r < R_2 \\ &V(r) = \infty, \quad r > R_2, \end{aligned} \tag{A1}$$

where for low temperatures we take $V_0 \to \infty$.

1. *f at High Temperatures*

It has been shown[2,45] that when thermal relaxation is rapid, the single-particle f in the high-temperature classical regime is, for all single-particle potentials $V(\vec{r})$,

$$f = \left| \iiint e^{-\beta V(\vec{r})} e^{i\vec{k}\cdot\vec{r}} d^3r \Big/ \iiint e^{-\beta V(\vec{r})} d^3r \right|^2 . \tag{A2}$$

For a spherically symmetric $V(r)$,

$$\sqrt{f} = \int_0^\infty e^{-\beta V(r)} r \sin(kr)\, dr \Big/ k \int_0^\infty e^{-\beta V(r)} r^2\, dr. \tag{A3}$$

Equation (A3) implicitly assumes that the particle's motion is well averaged in θ and ϕ during the lifetime of the γ ray. The calculation of Eq. (A3) with potential Eq. (A1) is straightforward, and it can be neatly expressed in terms of the f factors for hard-walled spherical cavities of radii R_1 and R_2; for the squared wine-bottle factor f_{swb} we obtain

$$\sqrt{f_{\mathrm{swb}}} = \frac{\sqrt{f(R_2)} - (1 - e^{-\beta V_0}) Q^3 \sqrt{f(R_1)}}{1 - (1 - e^{-\beta V_0}) Q^3} , \tag{A4}$$

where $Q = R_1/R_2$ and

$$\sqrt{f(R)} = [3/(kR)^2]\, (\sin kR/kR - \cos kR) . \tag{A5}$$

From the condition that the high-temperature approximation is valid when the thermal energy is much greater than the energy level separation, we find Eq. (A4) holds when $\beta\pi^2\hbar^2/8\, m(\Delta R)^2 \ll 1$.

The general dependence of f_{swb} on the parameters

is interesting. We see that f_{swb} correctly approaches $f(R_2)$ as Q or V_0 tend to zero. The temperature dependence is strikingly different from either the square well or harmonic behavior:

$$\beta V_0 \to 0 \quad f_{swb} \to f(R_2)$$
$$\beta V_0 \to \infty; \quad \sqrt{f_{swb}} \to [\sqrt{f(R_2)} - Q^3\sqrt{f(R_1)}]/(1-Q^3)\,. \tag{A6}$$

The asymptotic expression for f_{swb} at large βV_0 is smaller than for small βV_0, i.e., *f decreases at lower temperatures*. The decrease comes about because the central maximum forces the particle to larger average values of r as the temperature falls, and of course, the f factor is generally smaller for larger average displacements. The decrease at lower temperatures is illustrated by an extreme example: a tight-binding wine bottle, in which the particle is constrained to remain at a fixed value $r = R$ while averaging rapidly over the spherical angles. In this case $e^{-V(r)}$ has the form of a δ function, constant $\delta\,(r-R)$, and Eq. (A3) becomes

$$\sqrt{f} = \sin kR/kR. \tag{A7}$$

This expression, which is identical to that for a one-dimensional square well,[46] shows a spectrum of zeros at $kR = n\pi$ for $n = 1, 2\cdots$. The zeros arise from the interference of the radiation emitted from the various polar angles θ. Interference occurs in the more general Eq. (A4), although it is weaker if the flat bottom has a finite width.

2. *f at Low Temperature*

For the low-temperature limit $T = 0$, we must use the ground-state wave function to calculate

$$f_0 = \langle 0 \,|\, e^{i\vec{k}\cdot\vec{r}} \,|\, 0\rangle\,. \tag{A8}$$

For all spherically symmetric potentials the solution of the Schrödinger equation is[47]

$$\psi(r,\ \theta,\ \phi) = (N_{lm}/2\pi)P_l^m(\cos\theta)e^{im\phi}\,\chi(r)/r\,,$$

where $\chi(r)$ is a solution of the radial equation

$$-(h^2/2m)(d^2\chi/dr^2) + [l(l+1)/mr^2]\,\chi = \epsilon\,\chi. \tag{A9}$$

The ground state $n = 1$, $l = 0$ has simple harmonic solutions, for $R_1 < r < R_2$,

$$\chi(r) \propto \sin\alpha r;\ \cos\alpha r \tag{A10}$$

where $\alpha = (2mE/h^2)^{1/2}$. We will assume that the central potential V_0 is sufficiently large [Fig. 5(c)] to set the "exterior" solutions ($r < R_1$, $r > R_2$) to zero. Then we obtain, for the radial wave function in the ground state,

$$\chi(r)/r \propto (\sin\alpha r)/r. \tag{A11}$$

Calculating f_0 with the radial wave function [Eq. (A11)], the result is again expressible in terms of factors for simple spherical cavities:

$$\sqrt{f_0} = (\alpha/k)\frac{[A(R_2) - A(R_1)]}{[\alpha\Delta R - (\sin\alpha\Delta R)(\cos 2\alpha R_{av})]}\,,$$

where

$$A(R) = \tfrac{1}{2}[2\mathrm{Si}(kR) - \mathrm{Si}(kR + 2\alpha R) - \mathrm{Si}(kR - 2\alpha R)],$$
$$\mathrm{Si}(x) = \int_0^x (\sin x'/x')\,dx'\,. \tag{A12}$$

and $\Delta R = R_2 - R_1$, $R_{av} = \frac{1}{2}(R_1 + R_2)$. The factor at $T = 0$ for a hard-walled spherical cavity of radius R is

$$[f_0(R)]^{1/2} = [\alpha A(R)/k]\,(\alpha R - \tfrac{1}{2}\sin 2\alpha R)^{-1}. \tag{A13}$$

When $|kR \pm 2\alpha R|$ is not much larger than unity, the expression can be reduced to simpler form by the series expansion[48]

$$\mathrm{Si}(x) = x - \frac{x^3}{3\times 3!} + \frac{x^5}{5\times 5!}\cdots \tag{A14}$$

For $x \leq 1.8$, the first two terms give the sum to within 3%. Within this range we obtain solutions independent of k; for the simple cavity

$$\sqrt{f_0(R)} = 2(\alpha R)^3/3(\alpha R - \tfrac{1}{2}\sin 2\alpha R)\,, \tag{A15}$$

and for the wine bottle

$$\sqrt{f_0} = \frac{2[(\alpha R_2)^3 - (\alpha R_1)^3]}{3[\alpha\Delta R - (\sin\alpha\Delta R)(\cos 2\alpha R_{av})]}\,, \tag{A16}$$

when $|kR \pm 2\alpha R| \lesssim 1.8$. In Fig. 8 we present curves for the variation of f with well radius, for several values of ΔR, calculated according to Eq. (A12).

3. *Thermal Shift*

The thermal or second-order Doppler shift $\delta\nu$ for all potentials and temperatures, is given by[49]

$$\delta\nu/c = \delta E_\gamma/E_\gamma = \langle\epsilon\rangle/mc^2, \tag{A17}$$

where $\langle\epsilon\rangle$ is the thermal average kinetic energy

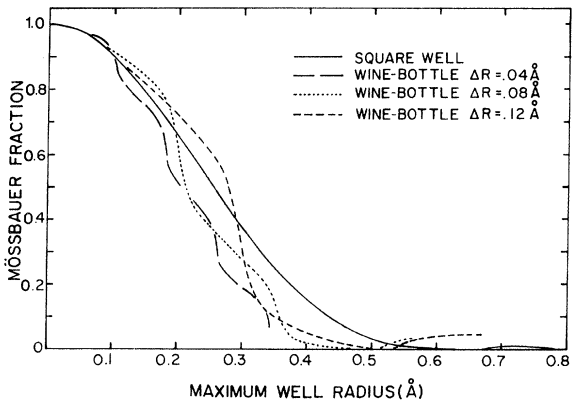

FIG. 8. Mössbauer fraction at $T = 0$ °K versus radius R_2 for a spherical square-well potential of various ΔR ($\Delta R = R_2 - R_1$).

of the particle. When kT is much larger than the level spacing, $\langle\epsilon\rangle = \frac{3}{2}kT$, but at low temperatures the finite level spacing causes deviation from classical behavior. For the squared wine-bottle potential, the kinetic energies will depend upon both quantum numbers n and l in Eq. (A8). However, if ΔR is small compared to R_{av} then the radial term dominates. For simplicity, we will here assume that the orbital terms are degenerate in energy. From the s-state solutions to Eq. (A9) we have

$$\epsilon_n = n^2\hbar^2\pi^2/8m(\Delta R)^2 = n^2\epsilon_1, \quad n = 1, 2 \ldots , \qquad \text{(A18)}$$

These levels now have degeneracies

$$g_n = \sum_{l=0}^{n-1} (2l+1). \qquad \text{(A19)}$$

The mean kinetic energy is an ensemble average

$$\langle\epsilon\rangle = \frac{-\partial \ln z}{\partial\beta} , \qquad \text{(A20)}$$

where z is the single-particle partition function

$$z = \sum_n g_n e^{-\beta\epsilon_n}. \qquad \text{(A21)}$$

Numerical calculations of δv were carried out for the energies and degeneracies given by Eqs. (A18) and (A19): The results for several choices of ϵ_1 are shown in Fig. 9. For each ϵ_1, the shifts are nearly temperature independent when $\beta\epsilon_1 > 1$, and they rapidly approach the classical shift at higher temperatures. An important feature of the curves is the asymptotic value at $T = 0$, a contribution that is superimposed on the temperature-independent chemical shift. Since ϵ_1 depends on ΔR and not on the mean well radius, the temperature dependences of δv and f can be used to determine the two parameters of the squared wine-bottle potential.

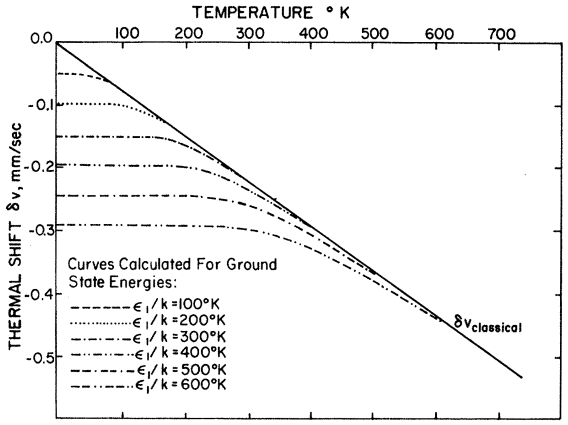

FIG. 9. Thermal shift (second-order Doppler shift) versus temperature for spherical wine-bottle potentials of various ground-state energy levels ϵ_1/k.

Real potentials of the wine-bottle variety have finite central maxima, in contrast to the simplification on which we have based our calculations. This complication will cause f to have a bizarre temperature dependence, tending to decrease at lower temperatures, as we have noted in the classical calculation. The decrease arises when the thermal average energy of the ion decreases to values comparable with the height of the central maximum and the ion becomes trapped in the spherical annulus. When this occurs, the ion is forced outward to larger radii, resulting in larger mean-squared displacements. If there are subsidiary minima[50] distributed around the spherical annulus in which the ion can be trapped, then a further surprising change will occur: At still lower temperatures f will rise again to relatively large values (~1) and remain large to 0 °K.

---

†Work supported by National Aeronautics and Space Administration Grant No. NGL 48-002-004.

*Permanent address: Physics Department, Technion Israel Institute of Technology, Haifa, Israel.

[1]R. M. Housley and F. Hess, Phys. Rev. 146, 517 (1966).

[2]J. G. Dash, D. F. Johnson, and W. M. Visscher, Phys. Rev. 168, 1087 (1968).

[3]D. P. Johnson and J. G. Dash, Phys. Rev. 172, 983 (1968).

[4]See *Handbook of Chemistry and Physics* (Chemical Rubber, Ohio), 44th ed., p. 670.

[5]R. M. Mecedo, W. Capps, and J. B. Wachtman, Jr., J. Am. Ceramic Soc. 47, 651 (1964).

[6]We are grateful to Dr. J. B. Gruber of Washington State University for supplying us with several excellent ThO_2 crystals.

[7]V. I. Neely, J. B. Gruber, and W. J. Gray, Phys. Rev. 158, 809 (1967).

[8]We are grateful to Dr. N. Gregory of the Department of Chemistry, University of Washington, for supplying us with the powder.

[9]We are grateful to T. Chikalla of Battelle N. W. at Richland, Wash., for preparing the pellet.

[10]Premium-grade $Co^{57}Cl_2$ solution obtained from New England Nuclear Corp., Boston, Mass.

[11]D. P. Johnson, G. A. Erickson, and J. G. Dash, Rev. Sci. Instr. 39, 420 (1968).

[12]R. M. Housely, N. E. Erickson, and J. G. Dash, Nucl. Instr. Methods 27, 29 (1964).

[13]R. M. Housley, Nucl. Instr. Methods 35, 77 (1965).

[14]D. P. Johnson, Ph.D. thesis, University of Washington, 1967 (unpublished).

[15]Powder obtained from New England Nuclear Corporation.

[16]B. L. Chrisman and T. A. Tumolillo, University of

Illinois Research in Nuclear Physics Technical Report No. 178, 1969 (unpublished).

[17]We are grateful to K. Coston of Arizona State University for supplying us with a modified version of the Tumolillo program.

[18]R. Ingalls, Phys. Rev. 188, 1045 (1969).

[19]D. N. Pipkorn (private communication).

[20]H. J. Lipkin, Ann. Phys. (N. Y.) 23, 28 (1963).

[21]P. G. Dawber and R. J. Elliott, Proc. Roy. Soc. (London) A273, 222 (1963).

[22]B. T. M. Willis, Proc. Roy. Soc. (London) A274, 122 (1963).

[23]W. M. Visscher, Phys. Rev. 134, A965 (1964).

[24]R. W. G. Wyckoff, in *Crystal Structures* (Interscience, New York, 1960), Vol. I, Chap. IV, pp. 2–4c; tables on pp. 13, 14a, 14c; illustration on p. 1.

[25]W. Low and D. Shaltiel, J. Phys. Chem. Solids 6, 315 (1958).

[26]F. Hund and W. Durchwachter, Z. Anorg. Allgem. Chem. 265, 67 (1952).

[27]J. B. Gruber (private communication).

[28]W. Elsasser, J. Phys. Radium 5, 625 (1934).

[29]E. Feenberg and K. C. Hammack, Phys. Rev. 75, 1877 (1949).

[30]J. E. Lennard-Jones and A. F. Devonshire, Proc. Roy. Soc. (London) A163, 53 (1937).

[31]C. Domb and J. S. Dugdale, in *Progress in Low Temperature Physics*, edited by C. J. Gorter (North-Holland, Amsterdam, 1957), Vol. II.

[32]F. D. Cramer, Rev. Pure Appl. Chem. 5, 143 (1955).

[33]G. Lombardo and R. O. Pohl, Phys. Rev. Letters 16, 1103 (1966).

[34]W. Low and M. Weger, Phys. Rev. 118, 1119 (1960).

[35]R. Ingalls, Phys. Rev. 133, A787 (1964).

[36]P. R. Edwards, C. E. Johnson, and R. J. P. Williams, J. Chem. Phys. 47, 2074 (1968).

[37]K. Ono, A. Ito, and Y. Syono, Phys. Letters 19, 620 (1966).

[38]H. H. Wickman, M. P. Klein, and D. A. Shirley, Phys. Rev. 152, 345 (1966).

[39]M. Blume and J. A. Tjon, Phys. Rev. 165, 446 (1968).

[40]Comment: Our model is essentially a one-axis case since we imagine relaxation time between two states giving equal and opposite EFG tensors. It is equivalent to the paramagnetic case where one considers the hfs in the case of relaxation between two electronic levels $m_s = \pm\frac{1}{2}$.

[41]F. S. Ham, Phys. Rev. 160, 328 (1967).

[42]H. R. Lieder and D. N. Pipkorn, Phys. Rev. 165, 494 (1968).

[43]J. Chappert, R. B. Frankel, A. Misetich, and N. A. Blum, Phys. Letters 28B, 406 (1969).

[44]F. S. Ham (private communication).

[45]H. J. Lipkin, Ann. Phys. (N. Y.) 26, 115 (1964).

[46]R. H. Dicke, Phys. Rev. 89, 472 (1953).

[47]See, for example, L. Landau and E. M. Lifshitz, *Quantum Mechanics* (Addison-Wesley, Reading, Mass., 1958).

[48]*Handbook of Mathematical Functions*, edited by M. Abramowitz and I. A. Stegun (U. S. Department of Commerce, National Bureau of Standards, Washington, D. C., 1964), Appl. Math. Ser. 55, p. 231.

[49]B. D. Josephson, Phys. Rev. Letters 4, 341 (1960).

[50]The spherically symmetric potentials we have assumed for these calculations are not physically realistic; as noted earlier, the actual potentials must reflect the local structure of the surrounding ions. A recent detailed study by R. E. Peierls and F. Goldstein [R. E. Peierls (private communication)] of substitutional impurities in a model fcc crystal has yielded results at some variance with those of the spherically symmetric wells. Although they find that the impurity f does have a displacement to lower values such as described in Ref. 2, they do not find the interference minima of the spherical model. The interference disappears because of the more complicated structure of the nonspherically symmetric potential which, after spatial averaging, is seen by the impurity as an effectively more diffuse repulsive wall.